Spinal Muscular Atrophy Associated with Progressive Myoclonic Epilepsy Is Caused by Mutations in *ASAH1*

Jie Zhou,[1] Marcel Tawk,[1] Francesco Danilo Tiziano,[2] Julien Veillet,[1] Monica Bayes,[3] Flora Nolent,[1] Virginie Garcia,[4] Serenella Servidei,[5] Enrico Bertini,[6] Francesc Castro-Giner,[3] Yavuz Renda,[7] Stéphane Carpentier,[4] Nathalie Andrieu-Abadie,[4] Ivo Gut,[3] Thierry Levade,[4,8] Haluk Topaloglu,[7] and Judith Melki[1,*]

Spinal muscular atrophy (SMA) is a clinically and genetically heterogeneous disease characterized by the degeneration of lower motor neurons. The most frequent form is linked to mutations in *SMN1*. Childhood SMA associated with progressive myoclonic epilepsy (SMA-PME) has been reported as a rare autosomal-recessive condition unlinked to mutations in *SMN1*. Through linkage analysis, homozygosity mapping, and exome sequencing in three unrelated SMA-PME-affected families, we identified a homozygous missense mutation (c.125C>T [p.Thr42Met]) in exon 2 of *ASAH1* in the affected children of two families and the same mutation associated with a deletion of the whole gene in the third family. Expression studies of the c.125C>T mutant cDNA in Farber fibroblasts showed that acid-ceramidase activity was only 32% of that generated by normal cDNA. This reduced activity was able to normalize the ceramide level in Farber cells, raising the question of the pathogenic mechanism underlying the CNS involvement in deficient cells. Morpholino knockdown of the *ASAH1* ortholog in zebrafish led to a marked loss of motor-neuron axonal branching, a loss that is associated with increased apoptosis in the spinal cord. Our results reveal a wide phenotypic spectrum associated with *ASAH1* mutations. An acid-ceramidase activity below 10% results in Farber disease, an early-onset disease starting with subcutaneous lipogranulomata, joint pain, and hoarseness of the voice, whereas a higher residual activity might be responsible for SMA-PME, a later-onset phenotype restricted to the CNS and starting with lower-motor-neuron disease.

Introduction

Childhood spinal muscular atrophy (SMA [MIM 253300, MIM 253550, MIM 253400, and MIM 271150]) is a clinically and genetically heterogeneous group of inherited neuromuscular disorders characterized by the degeneration of motor neurons of the spinal cord and leading to progressive atrophy of skeletal muscles and paralysis. The most frequent form is inherited as an autosomal-recessive trait resulting from mutations in survival of motor neuron 1 (*SMN1* [MIM 600354]).[1] The other forms of SMA are a genetically heterogeneous group of rare disorders differing by their mode of inheritance, the topography of the muscle deficit, or their association with other neurological abnormalities.

Progressive myoclonic epilepsy (PME) represents a heterogeneous group of epilepsies characterized by myoclonic and generalized seizures with progressive neurological deterioration. PME can occur as a pure form such as Lafora disease (MIM 254780), Unverricht-Lundborg type disease (MIM 254800), and myoclonic epilepsy with ragged red fibers (MERRF [MIM 545000]) or can be associated with neuronal ceroid lipofuscinosis (NCL [MIM 256730]), biopterin deficiency, and lysosomal-storage disorders.

A rare variant has been reported to associate lower-motor-neuron disease with progressive myoclonic epilepsy (SMA-PME) in childhood. This condition is inherited as an autosomal-recessive trait. Jankovic and Rivera[2] were the first to report this association as a clinically separate entity. Haliloglu et al.[3] reported two additional families affected by a syndrome characterized by severe and progressive myoclonic epilepsy and lower-motor-neuron disease proven by electrophysiological and muscle-biopsy findings. The facts that extensive metabolic investigations were normal and that *SMN1* mutations were ruled out indicate that the association between PME and SMA represents a separate clinical and genetic entity.

In this report, we combined exome sequencing and whole-genome scanning with the use of SNP microarrays to identify the genetic cause of SMA-PME in three unrelated families.

Subjects and Methods

Families

The first affected child, born from a first-degree consanguineous Turkish family (family D, Figure 1) consisting of three affected

[1]Institut National de la Santé et de la Recherche Médicale UMR 788, University of Paris 11, Biomedical Institute of Bicetre, Le Kremlin-Bicêtre 94276, France; [2]Istituto di Genetica Medica, Università Cattolica del Sacro Cuore, Roma 00168, Italy; [3]Centro Nacional de Análisis Genómico, University of Barcelona, Barcelona 080028, Spain; [4]Institut National de la Santé et de la Recherche Médicale UMR 1037, Centre de Recherches sur le Cancer de Toulouse, Université Paul Sabatier, Toulouse 31432, France; [5]Istituto di Neurologia, Università Cattolica del Sacro Cuore, Roma 00168, Italy; [6]Unit of Molecular Medicine, Department of Neurosciences, Ospedale Bambino Gesù Research Institute, Roma 00165, Italy; [7]Child Neurology Unit, Department of Pediatrics, Hacettepe University, Ankara 06100, Turkey; [8]Laboratoire de Biochimie Métabolique, Institut Fédératif de Biologie, Centre Hospitalier Universitaire de Toulouse-Hôpital Purpan, Toulouse 31432, France
*Correspondence: judith.melki@inserm.fr
DOI 10.1016/j.ajhg.2012.05.001.

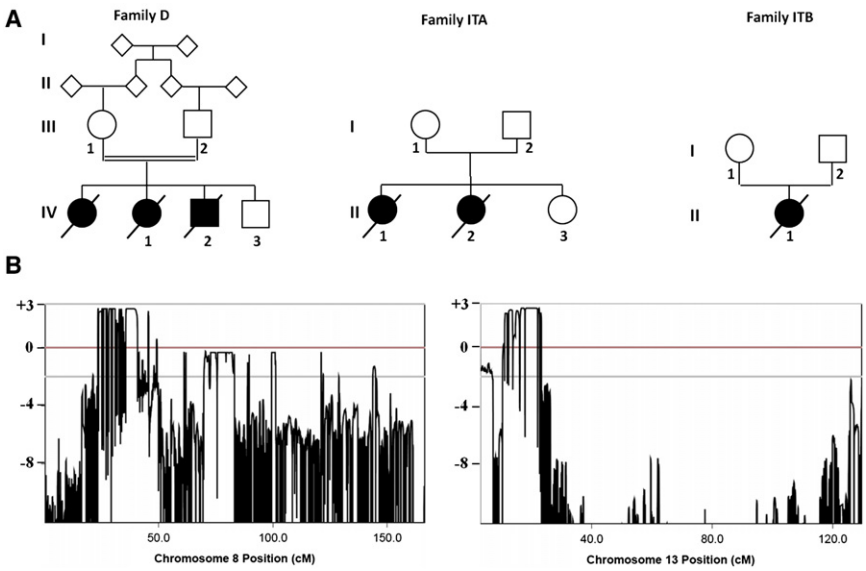

Figure 1. Pedigrees and Linkage Analysis in SMA-PME-Affected Families
(A) Pedigrees of SMA-PME-affected families. The numbers denote individuals whose DNA samples were available for genetic analysis. Linkage analysis and homozygosity mapping were performed in families D and ITA.
(B) Combined results of linkage analysis of families D and ITA show a maximum LOD score $Z_{max} = 2.7$ at $\theta = 0.0$. The *x* axis represents genetic distance in cM, and the *y* axis represents LOD scores.

siblings and one unaffected sibling, developed progressive walking difficulties, frequent falls, and a tremor in her hands from the age of 5 years. Early developmental milestones were normal, and she was able to walk at the age of 14 months. Physical examination revealed proximal weakness and muscular atrophy. A creatine kinase (CK) test was normal. Electromyography (EMG) showed a chronic denervation process. By the age of 7 years, she began to have brief myoclonic seizures without losing consciousness. An electroencephalograph (EEG) showed slow and sharp bilateral waves of 3–4 cycles/s. Repeated EEGs showed subcortical-myoclonic epileptiform abnormalities sensitive to hyperventilation. When the patient was 11 years old, muscle biopsy showed neurogenic atrophy but no changes suggestive of a mitochondrial disorder. The disease was progressive and caused recurrent lung infections. She died at the age of 13 years. The second and third affected children (IV-1 and IV-2, Figure 1,) had very similar symptoms, including myoclonic epilepsy and muscle weakness resulting from a denervation process. The disease course was progressive, and both died at 17 years of age.

In this family, lysosomal screening tests for hexosaminidase A, examination of peripheral blood leukocytes for a possible NCL, and mitochondrial-DNA mutational analysis for MERRF were negative. Fundoscopic examination, electroretinography, and skin biopsy were normal. *SMN1* copy number was normal. Brain magnetic resonance imaging (MRI) of the three affected siblings was normal.

The second family (family ITA, Figure 1) consisted of two affected sisters born to unrelated healthy Italian parents. They had normal motor and intellectual milestones. At 4 (II-1, Figure 1) and 5 years of age (II-2), they developed progressive muscle weakness of the lower and then upper limbs. Around age 12, both had generalized epileptic seizures, numerous brief episodes of loss of consciousness, and myoclonic jerks. Both affected children lost the ability to walk at 17 years of age. Both sisters showed mild facial weakness and difficulty swallowing, fasciculations of the tongue, muscle weakness, absent deep-tendon reflexes, severe scoliosis, and subsequent respiratory insufficiency. EMG and muscle biopsies showed a denervation process, and brain MRI was normal.

In the third family (family ITB, Figure 1), the affected girl (II-1) was born to unrelated healthy Italian parents. Early developmental milestones were normal. Progressive muscle weakness started at the age of 5 years. Around the age of 10 years, the girl began having brief episodes of loss of consciousness usually accompanied by myoclonic jerks of the upper limbs. When she was 11 years old, a neurological examination showed diffuse muscle atrophy, mild facial weakness and difficulty swallowing, and fasciculations of the tongue. The affected child died from pneumonia at the age of 15 years. EMG and muscle biopsy showed evidence of a denervation-reinnervation process. Brain MRI performed when she was 10 years old showed no significant abnormalities. Between the ages of 10 and 14 years of age, her EEG recordings showed normal background activity and paroxysmal activity that consisted—in frequent diffuse bursts—of sharp waves and poly-spike and wave complexes that were present both in conscious wakefulness and non-rapid-eye-movement sleep stages 1 and 2. Neither skin nor joint abnormalities were reported in these affected individuals. In accordance with the ethical standards of the institutional review boards at CPP Île de France, DNA samples from affected individuals and their parents were collected after written informed consent was given.

Genome-wide Linkage Analysis

Whole-genome SNP scanning was carried out according to the Affymetrix 250K GeneChip Mapping Assay manual. Multipoint linkage analysis and homozygosity mapping of SNP data applied to the whole genome were performed with Alohomora[4] and Merlin software[5] with the following parameters: autosomal-recessive inheritance, 100% penetrance, and a 1:1,000 disease gene frequency in the population.

Genome-Wide Human SNP Nsp/Sty Assay Kit 6.0 was used for copy-number examination of the *ASAH1* (MIM 613468) locus according to the Affymetrix SNP 6.0 array protocol. Copy-number variation (CNV) detection was performed by Birdseed in Affymetrix Genotyping console 4. A dataset of 90 HapMap samples was added for the determination of CNV.

Exome Sequencing

The Illumina TruSeq DNA Sample Prep kit v.1 and the NimbleGen SeqCap EZ Exome v.1 were used for library preparation and exome enrichment, respectively. In brief, genomic DNA (3–5 μg) was fragmented in a Covaris S2 instrument. Fragmented DNA was processed through enzymatic treatments of end repair, dA tailing, and ligation to Illumina's adapters. A 200–300 bp fraction was excised from an agarose gel, and the adaptor-ligated library was PCR amplified with Illumina PE primers for eight cycles. Products

(500 ng) were hybridized to the capture oligomers for 70 hr at 47°C. Biotinylated hybrids were captured, and the enriched fraction was eluted and amplified with 14 additional PCR cycles. The pre- and post-capture libraries were compared by quantitative PCR for the determination of the relative fold enrichment of the targeted sequences. The library was applied to an Illumina flow cell for cluster generation. Sequencing was performed on a Genome Analyzer IIx instrument with 75 bp paired-end reads according to Illumina's protocol.

Reads were aligned to the human reference genome sequence (UCSC hg19, National Center for Biotechnology Information [NCBI] build 37.3) via the Burrows-Wheeler Aligner (BWA) program.[6] Variants were selected with Samtools[7] and were then annotated with Annovar software.[8] Reads with a mapping quality score of at least 20 and at least 5× coverage were filtered against dbSNP v.131. Intron-exon junctions, nonannotated variants (including synonymous, nonsynonymous, and nonsense mutations) in coding regions, or short coding insertions or deletions were selected. The ratio of mutants to total reads was at least 20%. An autosomal-recessive model was applied. Finally, variants mapping to the candidate regions as determined by linkage analysis were selected.

Real-Time PCR Amplification of Genomic DNA

Real-time PCR amplification was conducted with the use of genomic DNA on a 7300 Real-Time PCR system (Applied Biosystems) with Power SYBR Green PCR Master Mix (Applied Biosystems). Genomic deletion was defined when the ratio of tested DNA to control DNA was equal to or less than 0.5. Real-time PCR amplification of each sample was performed in duplicate with primers within *ASAH1* exons 1, 2, or 14 (Table S1, available online). Albumin was used as an internal control (Table S1).

Reverse-Transcription-PCR Amplification

Total RNAs were extracted by the TRI Reagent LS method (Sigma). One microgram of RNA was used for synthesizing cDNA with the use of random primers according to the manufacturer's manual (SuperScript III Reverse Transcriptase, Invitrogen) in a final volume of 20 μl. Reverse-transcription PCR (RT-PCR) amplification was carried out with 1.5 mM $MgCl_2$, 0.6 U DNA Polymerase (Invitrogen), 0.2 μM of each primer, and 1 μl cDNA. After an initial denaturation cycle at 94°C for 5 min, 30 cycles were performed and consisted of denaturation at 94°C for 30 s, annealing at 60°C for 1 min, and extension at 72°C for 1 min; these cycles were followed by a final extension at 72°C for 7 min in an ABI 9700 Thermal Cycler (Applied Biosystems). RT-PCR products were separated by agarose gel electrophoresis and labeled with ethidium bromide.

For determining the effect of the mutation in exon 2 of *ASAH1* on transcripts, PCR-amplification analysis of single-strand cDNA was performed with a forward primer chosen in exon 1 and reverse primers in exons 4, 5, or 6 (Table S1). As an internal control for PCR amplification, β-actin cDNA was coamplified (Table S1). Sanger sequencing was performed from the PCR products.

Sanger Sequencing

PCR primer pairs were designed from genomic DNA to amplify exon 2 of *ASAH1* (Table S1). PCR amplification was carried out with 1.5 mM $MgCl_2$, 0.6 U DNA polymerase, 0.25 μM of each primer, and 100 ng DNA. After an initial denaturation cycle at 94°C for 5 min, 30 cycles were performed and consisted of denaturation at 95°C for 30 s, annealing at 60°C for 1 min, and extension at 72°C for 1 min; these cycles were followed by a final extension at 72°C for 7 min in an ABI 9700 Thermal Cycler. PCR products were then purified on P100 columns (Bio-Gel P-2 Gel fine, Biorad) and were sequenced with the forward or reverse primers and the Big Dye Terminator v.3.1 Cycle Sequencing Kit (Applied Biosystems). The sequencing reaction products were purified on G50 columns (Sephadex G-50 Superfine, GE Healthcare) and then migrated on an automated fluorescent DNA sequencer (ABI Prism 3100 Genetic analyzer, Applied Biosystems). The obtained DNA sequences were compared with published sequences (BLAST, NCBI).

Cloning of Mutant cDNA and Expression Studies of Acid Ceramidase

Cell Lines and Transfections

The cDNA of *ASAH1,* corresponding to transcript variant 1 (RefSeq accession number NM_177924), was kindly provided by Dr. J.A. Medin (University of Toronto, Canada) and subcloned into pcDNA5/TO (Life Technologies).[9] The c.125C>T mutation was introduced into wild-type (WT) cDNA after the removal of the BamHI-BsgI restriction fragment flanking the mutation and the ligation of a BamHI-BsgI restriction fragment derived from RT-PCR of the affected individual's RNA with primers provided in Table S1. The plasmid was transformed into DH5α-$T1^R$ *E. coli* (Invitrogen). Sequencing of mutant cDNA confirmed the insertion of the mutation and the lack of any other sequence changes. The Farber fibroblast cell line is a SV40 large T-transformed cell line derived from a Farber-disease-affected individual (MIM 228000) with an acid-ceramidase-activity level that is less than 3.5% of the control value.[10,11] Cells were grown in a humidified 5% CO_2 atmosphere at 37°C in DMEM medium containing 10% fetal calf serum and Glutamax (Life Technologies). Fibroblasts were transfected with the use of either Lipofectamine 2000 (Life Technologies) or Superfect (QIAGEN). The pCMV/LacZ vector was cotransfected with WT or mutant *ASAH1* cDNA for the evaluation of the efficiency of transient expression through bacterial β-galactosidase activity. Acid-ceramidase activity was normalized to the protein level and bacterial β-galactosidase activity. Cotransfection of both nonrecombinant pcDNA5/TO and pCMV/LacZ vectors was used as a blank.

Enzymatic Assays

Acid-ceramidase activity was assayed with Rbm14-12; bacterial β-galactosidase activities were determined with 4-methylumbelliferyl-β-D-galactopyranoside as a substrate (Sigma) as previously reported.[9,12,13]

Quantitation of Ceramide

After extraction of lipids, ceramide levels were determined with the use of *E. coli* diacylglycerol kinase and [γ^{32}P]-ATP as previously described.[14]

Immunoblotting Experiments

Pellets of transfected cells were resuspended in 0.2 ml of ice-cold lysis buffer (Cell Signaling Technology) and immunoblotted with a rabbit polyclonal acid-ceramidase antibody (kindly provided by Drs. K. Sandhoff and H. Schulze, Bonn, Germany). Immunoreactive proteins were detected with enhanced chemiluminescence (Pierce). The β-actin monoclonal antibody (Cell Signaling Technology) was used as an internal control for loading. The density of the bands was quantified with ImageJ (National Institutes of Health).

Knockdown of *ASAH1* in Zebrafish with Antisense Morpholino Oligonucleotides

Embryos were staged and cared for according to standard protocols.[15]

Injections of Antisense Morpholino Oligonucleotides

Antisense morpholino oligonucleotides (MOs) were purchased from Gene Tools. *asah1b*-MO (Table S1) was designed to target the 5′ UTR of *asah1b* mRNA (RefSeq NM_200577). The control "mismatch" morpholino (Table S1) had five nucleotides altered along its sequence. Morpholinos were dissolved in water to a final concentration of 0.6 mM; 1 nl of morpholino was injected into 1- to 4-cell-stage embryos as previously described.[16]

Immunohistochemistry

For immunostaining, embryos were fixed in 4% paraformaldehyde and stained as whole mounts. The acetylated-tubulin antibody (Sigma) was used at a 1:1,000 dilution. The znp-1 antibody (Developmental Studies Hybridoma Bank) was used at a dilution of 1:75. Primary antibodies were detected with appropriate secondary antibodies conjugated to Alexa 488 (Molecular Probes) at a 1:200 dilution.

Confocal Image Analysis

Image acquisition was performed with a Zeiss confocal microscope and Zeiss LSM imaging software. Images were captured in z sections at 2 μm increments. Axonal-branch analysis was performed offline with the ImageJ plugin NeuronJ and Adobe photoshop. Analysis was restricted to fascicles ventral to the spinal cord because labeling of spinal neuropil precluded the accurate examination of dorsal processes. Thus, axon branches of the rostral and caudal primary motor neurons were included for analysis. Branch patterns of five consecutive somites were analyzed per fish (three are presented for each group).

Acridine-Orange Staining

Living zebrafish larvae were anesthetized with Tricaine (Sigma-Aldrich), incubated in a solution of 3 μg/ml acridine orange (Sigma-Aldrich) with Tricaine for 30 min, and then washed. For imaging, fish were embedded in 1.2% low-melting agarose.

Statistics

Mean values and standard deviations (SDs) were calculated with Microsoft Excel. Statistical analysis was performed with a Student's t test. p values < 0.05 were considered as significant.

Enzymatic assays and quantization of ceramide are described above.

Results

Genome-wide SNP Genotyping and Exome Sequencing Identify *ASAH1* Mutations in SMA-PME

To identify the disease locus, we conducted genome-wide SNP genotyping by using the 250K NspI microarrays in the two multiplex families (families D and ITA, Figure 1). Multipoint linkage analysis of SNP data was performed for each family, and homozygosity mapping was performed for the consanguineous family (family D). Combining linkage data from the two multiplex families revealed two overlapping loci in chromosomal regions 8p22 and 13q12; each locus had a maximum LOD score of $Z_{max} = 2.7$ at $\theta = 0.0$ (Figure 1). The sizes of the disease loci in chromosomal regions 8p22 and 13q12 were 8.38 Mb and 4.46 Mb, respectively. The recombinant events were observed between rs1510424 and rs7845953 (chr8: 14,450,366–22,828,463; human genome build 37.3) and between rs6490964 and rs2479781 (chr13: 25,196,912–29,653,083). According to Map viewer (NCBI), these intervals contained 97 annotated genes. We performed Sanger sequencing of exons and intron-exon junctions of candidate genes chosen on the basis of their position and function. No mutations in *ATP6V1B2* (MIM 606939), *EGR3* (MIM 602419), *LGI3* (MIM 608302), *MTIF3*, or *NUPL1* (MIM 607615) were found in the affected individuals.

We then performed exome sequencing by using the DNA sample of one affected individual per family (IV-1 in family D, II-2 in family ITA, and II-1 in family ITB; Figure 1). The median coverage of the targeted exomes was 62×, 71×, and 73× in the affected individuals from families D, ITA, and ITB, respectively. Nonannotated variants mapping to the two candidate regions as determined by linkage analysis were selected. As a result, only 24, 23, and 26 variants remained candidates in affected individuals from families D, ITA, and ITB, respectively. *ASAH1*, located on chromosome 8, was the only gene carrying nonannotated variants shared by the three unrelated affected individuals. The same missense mutation (c.125C>T [p.Thr42Met]; RefSeq NM_177924.3) in exon 2 of *ASAH1* was found in the three affected individuals. Sanger sequencing of DNA samples confirmed that the mutation was homozygous (or hemizygous) in the three affected persons (Figure 2). The p.Thr42Met missense substitution occurred at an evolutionarily conserved amino acid among different species (Figure S1). This mutation was absent in 95 ethnically matched controls. c.125C>T was found at a very low frequency (2 out of 10,756 alleles) in the current Exome Variant Server database (ESP5400). The possible impact of the p.Thr42Met substitution on the function of acid ceramidase was calculated with Polyphen-2 software.[17] This substitution is predicted to be damaging on the basis of its high score (0.969). Segregation analysis of the mutation was performed in the three families. In families D and ITA, both parents were heterozygous and affected siblings were homozygous for this missense mutation (Figure 2). In family ITB, the mother was heterozygous, whereas the father harbored only a WT allele, suggesting either an inherited or de novo deletion occurring at this locus (Figure 2). We performed real-time PCR on DNA from the affected individual in family ITB by using primers located in exons 1, 2, and 14 of *ASAH1*. A heterozygous deletion was observed in both the affected child and her father, indicating that the affected child was compound heterozygous for the c.125C>T mutation inherited from the mother and for a whole-gene deletion inherited from her father (data not shown). To refine the size of the deletion found in the affected individual of family ITB, we performed pangenomic analysis of her DNA by using the Genome-Wide Human SNP Array 6.0 that had an intermarker distance of less than 1 kb. A 55 kb heterozygous deletion was found on chromosome 8

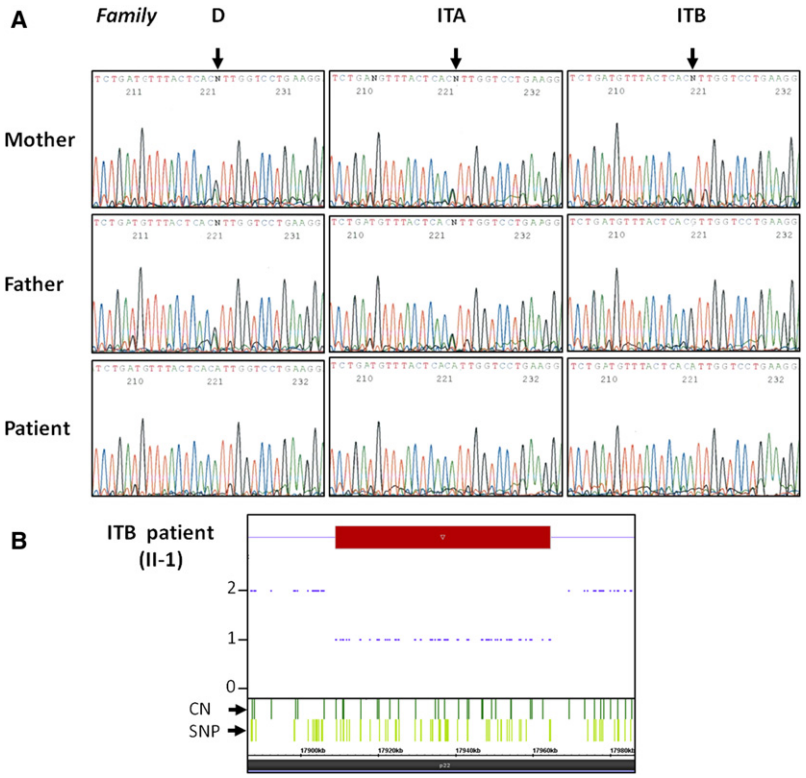

Figure 2. *ASAH1* Mutations Identified in SMA-PME-Affected Families

(A) Sanger sequencing of *ASAH1* exon 2 (genomic DNA) shows (1) a homozygous (or hemizygous) c.125C>T mutation in affected individuals of the three families (arrow); (2) a heterozygous c.125C>T mutation in both parents of families D and ITA and the mother of family ITB; and (3) a WT allele only in the father of family ITB. Reverse strands are shown.

(B) Copy-number and SNP analysis of the affected child in family ITB shows a heterozygous deletion of the whole gene. Dots indicate copy number and SNP copy number (1 or 2). Vertical bars indicate copy number (dark green) or SNPs (light green). The horizontal red rectangular box indicates the physical position of the heterozygous deletion.

from position 17,909,063 to 17,964,559 (Hg 19) and included 24 copy-number and 51 SNP probes (Figure 2). This deletion involves *ASAH1* only. Among the 51 SNPs mapping to the deleted region, 18 of them had a minor allele frequency (MAF) >5% and revealed an identical haplotype covering 31 kb in the affected individuals of the three families. These data suggest that the c.125C>T mutation occurred on a common ancestral allele.

Because the c.125C>T mutation involves the last nucleotide of *ASAH1* exon 2, binding sites for specific serine-and arginine-rich proteins might be modified. In silico analysis was performed with the ESEfinder program.[18] The mutation results in a higher score for the SC35 binding site. To determine whether abnormal splicing might occur in vivo and whether the mutation might result in aberrantly spliced products, we performed RT-PCR analysis of *ASAH1* from RNA extracted from blood leukocytes of the affected individual from family ITB. RT-PCR products from exon 1 to 4, 5, or 6 did not show any size difference between the affected individual and controls (Figure S1). Sequence analysis revealed that, compared to those of the controls, the RT-PCR products of the affected individual did not show any splice changes, indicating that this mutation does not affect the splicing process of *ASAH1* exon 2 in the cell type analyzed no matter which transcript variant it contains (isoform 1 or 2, Figure S1 and data not shown). To determine the pattern of expression of *ASAH1* transcripts, we performed RT-PCR analysis in various tissues, including lymphoblastoid cell lines and spinal cord, skeletal-muscle, and liver tissue. The *ASAH1* transcript was expressed in all tissues examined (Figure S1).

The p.Thr42Met Missense Substitution Results in Acid-Ceramidase Deficiency

Because cell cultures from SMA-PME-affected individuals were not available, WT and c.125C>T mutant *ASAH1* cDNAs were cloned into the pcDNA5/TO expression vector for functional studies. In order to assess the functional effect of the observed *ASAH1* missense mutation, we transfected recombinant vectors into immortalized fibroblasts derived from a Farber-disease-affected individual with a very severe acid-ceramidase activity (less than 3.5% of the control value).[10] WT or mutant *ASAH1* cDNA was cotransfected with the pCMV/LacZ vector. Acid-ceramidase activity was then normalized to the protein level and bacterial β-galactosidase activity. As shown in Table 1, transient expression of the mutant cDNA revealed that its acid-ceramidase activity was lower than that of the WT cDNA (i.e., it was about 32% of the control value). Similar results were observed with Superfect or Lipofectamine 2000 for transfection experiments (data not shown).

To directly assess the enzyme activity toward its natural substrate, i.e., ceramide, in living cells, we then examined whether the expression of the mutated cDNA in fibroblasts from a Farber-disease-affected individual could result in clearance of the accumulated substrate. Transient expression of either the WT or mutated sequence led to a marked (and similar) reduction of the ceramide storage (Table 1).

We performed immunoblotting experiments to characterize the WT and mutant proteins in human cells. Farber fibroblasts were transiently transfected with WT or c.125C>T mutant *ASAH1* cDNAs, and acid ceramidase was analyzed by immunoblot analysis (Figure 3). The substitution affects neither the level of the precursor form nor its processing. However, the α-subunit amount was mildly lower than the β-subunit amount.

Table 1. Acid-Ceramidase Activity and Ceramide Content in Farber Fibroblasts Expressing the p.Thr42Met Substitution

Transfected with:	Acid-Ceramidase Activity (pmol/h/mg)	Acid Ceramidase/ β-Galactosidase × 100	Ceramide Content (pmol/mg)
Nothing	278		18,543
Transfection agent only	961	0.8	17,141
Empty pcDNA5/TO	528	5.2	19,206
pcDNA5/TO-ASAH1	14,194	90.9	5,401
pcDNA5/TO-ASAH1-C2	16,333	137	3,372
pcDNA5/TO-ASAH1-C3	18,694	176	4,460
pcDNA5/TO-ASAH1-P4	5,194	37.7	5,250
pcDNA5/TO-ASAH1-P6	5,417	53.8	4,413

Farber cells were cotransfected in the presence of lipofectamine with a vector encoding LacZ and pcDNA5/TO vectors carrying *ASAH1* cDNA or not, and they were cultured for 48 hr. The pcDNA5/TO-ASAH1, pcDNA5/TO-ASAH1-C2, and pcDNA5/TO-ASAH1-C3 plasmids carry the WT sequence, whereas the pcDNA5/TO-ASAH1-P4 and pcDNA5/TO-ASAH1-P6 plasmids carry the mutant (c.125C>T) sequence. Acid-ceramidase and bacterial β-galactosidase activities and total ceramide content were determined on cell lysates as described in the Material and Methods. Acid-ceramidase activity is expressed as pmol/h/mg of protein, and ceramide level is expressed as pmol/mg of protein. Each determination was performed in duplicate. Note that the acid-ceramidase activity and ceramide content in normal fibroblasts average 7,000–9,000 pmol/h/mg and 1,000–2,500 pmol/mg, respectively.

Knockdown of *ASAH1* in Zebrafish Embryos Leads to Defective Motor Neurons

To analyze ASAH1 function in vivo, we used zebrafish as a model and designed for the *ASAH1* ortholog, *asah1b*, a translation-blocking antisense MO (*asah1b*-MO) that targets regions in the 5′ UTR of the mRNA.[16] *Asah1b* has the highest degree of homology (60%) with the ASAH1 preprotein (RefSeq NP_808592), particularly at the N-terminus, the region specific to the preprotein (variant 1). Embryos injected with 0.6 pmole of a 5 base mismatch control MO (referred to as "control 5 mis MO" below) were indistinguishable from uninjected, WT embryos ($n = 42$; Figures 4A and 4B). However, by 48 hr postfertilization (hpf), embryos injected with *asah1b*-MO (0.6 pmole) exhibited defects, including a curved body ($n = 50$; Figure 4C). To assess whether the general integrity of the embryos was affected, we analyzed cell death in living fish by incubation in acridine orange,[19] a dye that stains nucleic acids in dying cells. Comparison of morphants with both controls at 48 hpf demonstrated a significant increase in apoptosis in the spinal cord of morphants ($n = 8$ embryos for each group; WT versus control 5 mis MO: $t = 1.70$ and $p = 0.12$; *asah1b*-MO versus WT: $t = 11.7$ and $p < 0.0001$; *asah1b*-MO versus control 5 mis MO: $t = 9.87$ and $p < 0.0001$) (Figures 4D–4G), whereas no increase in cell death was detected elsewhere. These data suggest that neurons indeed degenerate in the spinal cord of asah1b morphants, whereas the general integrity of these embryos remains intact.

We next wished to determine whether asah1b could be involved in motor-axon development. To this end, we abrogated asah1b expression throughout early development with antisense MOs. We looked specifically at the primary motor neurons, which are few in number (typically three per somite), that undergo axonogenesis at 17 hpf and innervate the majority of muscle fibers in a given territory. To assess the developmental impact of asah1b reduction on axons of primary motor neurons, we used znp1 antibodies, panspecific markers of primary motor axons.[20] Although motor-axon branches of control-5-mis-MO-injected fish were similar to those of WT fish at 48 hpf (Figures 4H–4L), striking changes occurred in the asah1b morphants. Here, although motor axons appeared to be shorter in the morphants, the difference was not significant; however, there was a striking difference in the number of collateral branches in the asah1b morphants ($n = 25$ fascicles in six different embryos for each group; WT [18 ± 1.59 branches per fascicle (bpf)] versus control 5 mis Mo [17.8 ± 1.5 bpf and $p = 0.821$]; WT versus *asah1b*-MO [6.06 ± 2.2 bpf and $p < 0.0001$]; control 5 mis MO versus *asah1b*-MO [$p < 0.0001$]) (Figures 4K, 4L, 4M, and 4Q). To investigate whether the defect observed here was specific to motor-neuron axonal branching or was common to axonal projections in general, we used the acetylated-tubulin antibody, a microtubule marker that labels axonal projections. At 48 hpf, the posterior lateral line nerve (PLLn) had already reached the tip end of the tail in both controls and asah1b morphants (Figures 4N–4P). Thus, asah1b is required specifically for motor-neuron axonal branching (and probably for other spinal-cord neurons) but does not affect peripheral projections, at least as indicated by the PLLn. This also shows that there was no general delay in the development of the morphants compared with controls.

To confirm whether the morphant phenotype resulted from either knockout or knockdown of *Asah1b,* we determined the acid-ceramidase activity and ceramide content of zebrafish embryos (Table 2). Comparison of morphants with control zebrafish embryos revealed a significant decrease but not abrogation of acid-ceramidase activity in morphants (mean of 26%) without affecting ceramide content, indicating that antisense MOs resulted in knockdown of *Asah1b* in zebrafish. These data are consistent with those found in transfected human cells and

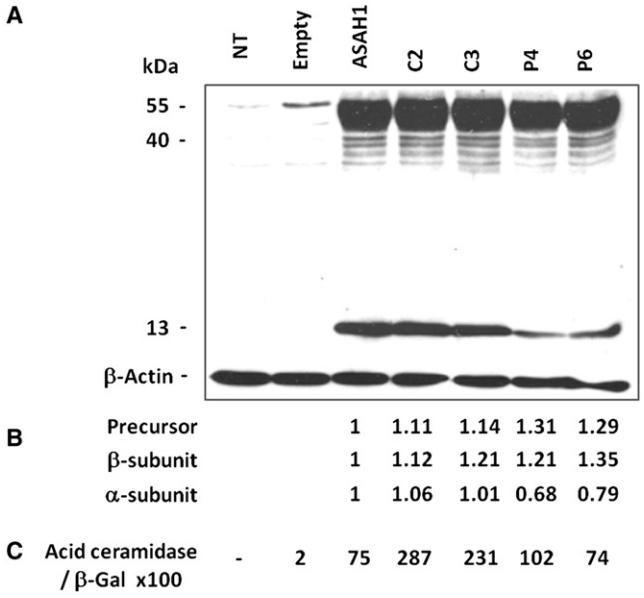

Figure 3. Immunoblot Analysis of ASAH1
(A) Farber fibroblasts were either not tranfected ("NT") or cotransfected with LacZ and pcDNA5/TO expression vectors carrying the *ASAH1* cDNA or not ("Empty"). The pcDNA5/TO-ASAH1 ("ASAH1"), pcDNA5/TO-ASAH1-C2 ("C2"), and pcDNA5/TO-ASAH1-C3 ("C3") plasmids carry the WT sequence, whereas the pcDNA5/TO-ASAH1-P4 ("P4") and pcDNA5/TO-ASAH1-P6 ("P6") plasmids carry the mutant (c.125C>T) sequence. Forty-eight hours later, cell extracts were analyzed by immunoblotting with acid-ceramidase and β-actin antibodies.
(B) The density of the bands corresponding to the precursor form (55 kDa), the β-subunit (40 kDa), and the α-subunit (13 kDa) of acid ceramidase was normalized to that of β-actin and compared to those of the WT protein ("ASAH1"). Note the reduced amount of the α-subunit in cells transfected with mutant cDNA.
(C) The acid-ceramidase and bacterial β-galactosidase enzyme activities were determined on the same cell lysates as described in Table 1.

demonstrate that asah1b plays an essential role in motor-neuron axonal branching and in the survival of spinal-cord neurons.

Discussion

Genome-wide linkage analysis combined with exome sequencing in three families affected by childhood SMA-PME allowed us to identify *ASAH1* mutations as responsible for this disease entity.

The main clinical feature of this condition is the onset of motor deficits at the age of 3 years after normal developmental milestones. Progressive muscle paralysis is caused by the involvement of lower motor neurons and is determined by EMG and/or muscle biopsy. Myoclonic epilepsy is then observed and is generally resistant to conventional therapy. The disease course is progressive and leads to respiratory muscle involvement and severe handicap or death occurring before 20 years of age. Neither skin nor joint abnormalities were noticed, and brain MRI was normal. In families D and ITA, affected children are homozygous for the c.125C>T missense mutation. In family ITB, the affected child carries the c.125C>T missense mutation and a deletion of the whole gene. The deleterious effect of the p.Thr42Met missense substitution on acid-ceramidase activity and the marked defect of motor-neuron axonal branching associated with a significant increase in apoptosis in the spinal cord of asah1b morphants further support the finding that *ASAH1*mutations are responsible for SMA-PME.

Mutations of the same gene are responsible for Farber disease, a very rare autosomal-recessive condition resulting from marked reduction or complete lack of lysosomal acid-ceramidase activity.[21] Farber disease manifests most commonly between 2 weeks and 4 months of age and has a unique triad of clinical manifestations: (1) painful and progressively deformed joints, (2) subcutaneous nodules, particularly near the joints and over pressure points (lipogranulomata), and (3) progressive hoarseness due to laryngeal involvement. The liver, spleen, lungs, and heart are often involved, and the nervous system can show accumulation of ceramides and gangliosides in the neurons of the brain and spinal cord. The illness is progressive and often leads to death at a mean age of 1.45 years in the classical form. A minority of affected infants survive beyond 5 years of age. Diagnosis is confirmed by an acid-ceramidase assay or by morphologic and/or biochemical studies of biopsy or autopsy tissues.

None of the individuals with SMA-PME reported here have the main clinical manifestations of Farber disease. In addition, the first symptoms of SMA-PME appear later (>3 years of age) and are restricted to the CNS, and death occurs after 12 years. This might explain why Farber disease and SMA-PME have not been suspected to be allelic conditions so far.

Data on almost 80 Farber-disease-affected individuals in a variety of ethnic groups have been reported.[21] In vitro residual activity of acid ceramidase is less than 10% in Farber disease. The ceramide that accumulates in Farber disease is primarily located in the lysosomes. Turnover studies have shown that it results from the impaired capacity of acid ceramidase to hydrolyze the ceramide generated during the degradation of complex sphingolipids. However, Samuelsson and Zetterstrom[22] reported on mildly affected individuals in whom liver, lung, or brain ceramide levels were normal. Therefore, the role of ceramide accumulation in the disease pathogenesis remains unclear. In SMA-PME-affected individuals, we found that the c.125C>T mutation causes residual acid-ceramidase activity to be about one-third of that of normal cells. Immunoblotting experiments showed that the α-subunit amount was mildly lower than the β-subunit amount, suggesting that the c.125C>T mutation that occurs within the α-subunit might affect its stability and result in reduced acid-ceramidase activity. Neither the c.125C>T mutation nor the whole-gene deletion has been reported in Farber disease. A homozygous missense substitution (p.Tyr36Cys) has already been reported in

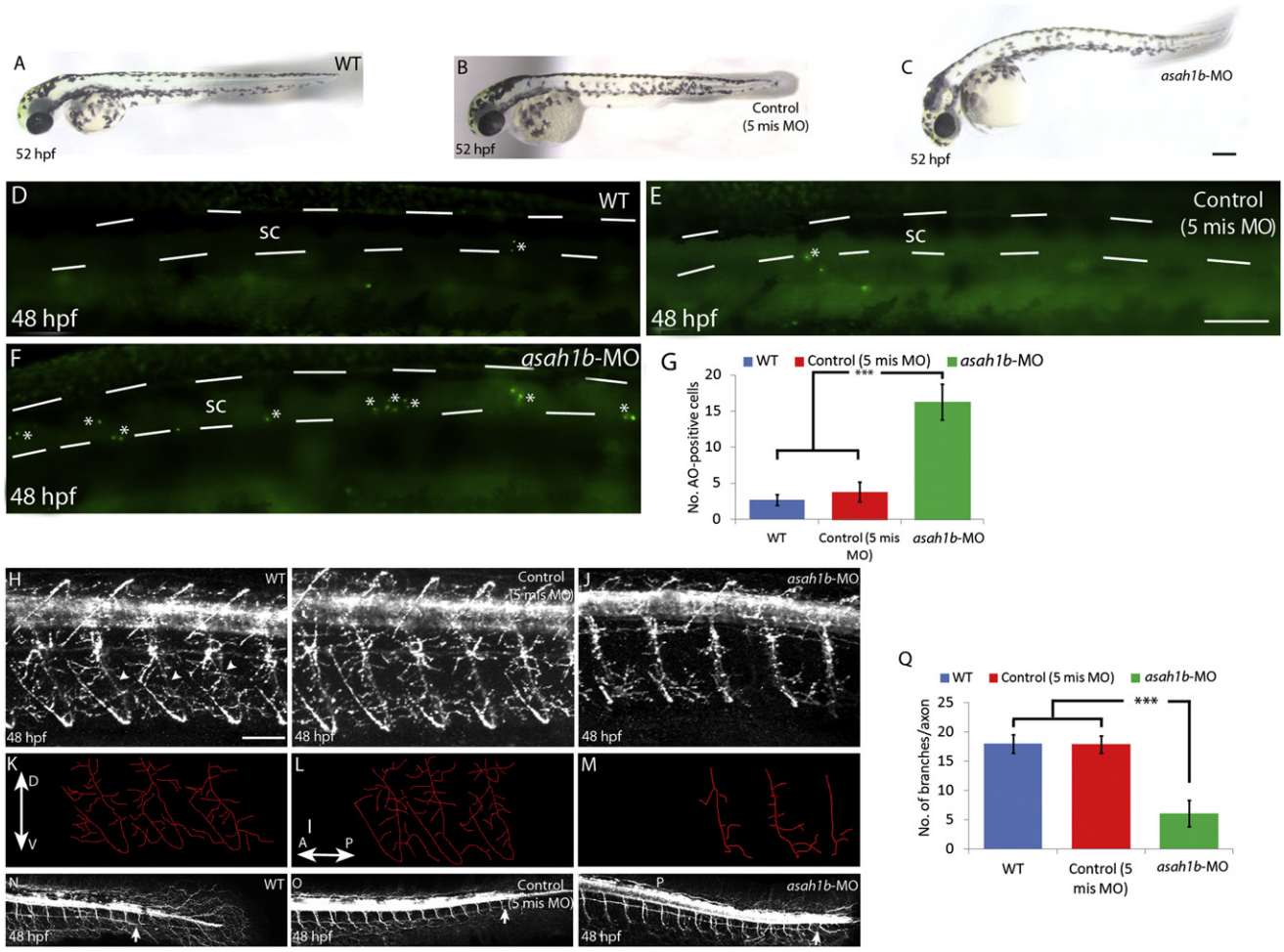

Figure 4. Morpholino Knockdown of *asah1b* in Zebrafish

(A–C) Morphology of living embryos at 52 hpf. WT embryos, control-5-mis-MO-injected embryos, and embryos injected with 0.6 pmole of *asah1b*-MO (asah1b morphants) are shown. Note the curved body shape that asah1b morphants show in comparison to the body shape of both controls. Views are lateral, and the dorsal sides are at the top. The scale bar represents 200 μm.

(D–F) Side views of 48 hpf living zebrafish embryos stained with acridine orange (D); some single acridine-orange-positive neurons are depicted by asterisks in WT embryos, control-5-mis-MO-injected embryos (E), or asah1b morphants (F). Asah1b morphants show substantial cell death in the spinal cord (dashed lines), whereas both controls show only a low, basal number of apoptotic cells. The scale bar represents 100 μm. The following abbreviation is used: sc, spinal cord.

(G) Bar chart depicting the mean number (± SD) of acridine-orange-positive cells per surface unit for WT (2.66 ± 0.74), control 5 mis MO (3.83 ± 1.34), and asah1b morphants (16.3 ± 2.5) at 48 hpf. Data represent mean ± SD. ***$p < 0.0001$.

(H–M) The *asah1b* morpholino decreases motor-axon collateral formation. Lateral views of znp1-antibody staining of controls (H and I) and asah1b morphants (J) are shown at 48 hpf. znp1 labels motor axons (H, arrowheads). Tracings of motor-axon tracts ventral to the spinal cord (K–M) are derived from panels directly above. Scale bars represent 50 μm. The following abbreviations are used: D, dorsal; V, ventral; A, anterior; and P, posterior.

(N–P) Lateral views of acetylated-tubulin-expressing axons of the PLLn (arrow) in WT, control-5-mis-MO-injected embryos, and asah1b morphants at 48 hpf. Axonal growth is similar in all groups; the PLLn reaches the tip end of the tail (arrows, n = 10 per group).

(Q) Bar chart depicting the mean number (± SD) of axon branches per fascicle for WT (18 ± 1.59), control-5-mis-MO-injected embryos (17.8 ± 1.5), and asah1b morphants (6 ± 2.2) at 48 hpf. Compared with both controls, Asah1b morphants show a significant decrease in axonal branching. ***$p < 0.0001$.

a classical form of Farber disease leading to less than 5% of normal acid-ceramidase activity.[21] Although the position of p.Tyr36Cys is close to the p.Thr42Met substitution found in SMA-PME-affected individuals, the marked difference in the level of acid-ceramidase activity in Farber disease and SMA-PME might account for distinct and later-onset clinical SMA-PME phenotypes.

Importantly, in addition to the unique triad of clinical manifestations of Farber disease, lower-motor-neuron involvement characterized by hypotonia and muscular atrophy with diminished or lack of deep-tendon reflexes was observed in 11 out 80 individuals with the classical form of Farber disease at late stages of disease progression (type 1).[21] EMG showed signs of denervation. Salaam-type seizures or infantile spasms were reported in two affected individuals. The nervous system was abnormal in all autopsied affected persons; an accumulation of storage material was found in the neuronal cytoplasm,

Table 2. Acid-Ceramidase Activity and Ceramide Content in Control and Farber Fibroblasts and in WT and Morphant Zebrafish Embryos

	Acid-Ceramidase Activity (pmol/h/mg)	Acid-Ceramidase Activity (%)	Ceramide Content (pmol/mg)
Experiment 1			
Control fibroblasts	8,556		958
Farber fibroblasts	267	3.1%	8,004
Experiment 2			
WT zebrafish-1	5,172		1,123
MO zebrafish-1	1,324	25.6%	637
MO zebrafish-2	561	10.8%	786
Experiment 3			
WT zebrafish-2	7,319		885
MO zebrafish-3	3,064	41.9%	786

Each determination was performed in duplicate. The residual acid-ceramidase activity (%) is shown as the ratio of mutant to WT activity within each set of experiments. The following abbreviations are used: WT, wild-type; and MO, morphant.

particularly in the anterior horn cells of the spinal cord but also in the brain-stem nuclei, basal ganglia, cerebellum, retinal ganglion cells, and cortical neurons. These data indicate that the CNS is progressively involved in Farber disease. Consistent with these data, the fact that spinal motor neurons show axonal-branching defects indicates a marked and early-onset vulnerability of motor neurons in response to ASAH1 knockdown in zebrafish embryos.

Our findings strongly suggest that although a dramatic reduction of acid-ceramidase activity leads to Farber disease, a very severe and early-onset disease characterized by an involvement of joints, skin, and laryngeal tissues and progressive neurological deterioration, a milder reduction of enzymatic activity leads to a later-onset of symptoms restricted to spinal-cord motor neurons and other areas of the CNS. Several therapeutic strategies have been undertaken for Farber disease. Allogeneic bone-marrow transplant (BMT) has been performed in a 9.5-month-old child with minimally symptomatic Farber disease.[23] Ceramidase activity in peripheral-blood leukocytes increased from 6% to 44% by 6 weeks after BMT. By 6 months after BMT, the subcutaneous lipogranulomata, contractures and joint pains, and hoarseness of the voice had completely resolved. However, the affected individual developed progressive hypotonia, muscle weakness, loss of head control, inability to sit unassisted, flexion contractures, opisthotonus, and tongue fasciculations.[23] These features are consistent with the occurrence of lower-motor-neuron involvement, the main clinical feature found in SMA-PME-affected individuals. Although the p.Thr42Met substitution results in a mild deficiency of acid-ceramidase activity, it is able to normalize the ceramide level in Farber cells. This result suggests that the pathogenic mechanism underlying the CNS involvement observed in SMA-PME is probably unrelated to ceramide accumulation in affected cells. However, the possibility that, in specific cell types such as motor neurons, this particular substitution results in changes of some ceramide (or other sphingolipids) molecular species not detected by the applied methods cannot yet be ruled out.

Medin et al.[11] reported that the introduction of WT human acid-ceramidase cDNA with a recombinant oncoretroviral vector into Farber-disease-cultured fibroblasts restored enzyme activity completely and normalized ceramide levels. Importantly, this study demonstrated that transduced cells allowed diffusion of this enzyme into the culture medium and that this activity could be taken up subsequently into unmodified cells. More recently, a preclinical Farber-disease gene-therapy study employing a lentiviral vector has been performed on nonhuman primates. Acid-ceramidase activity was detected above normal levels in peripheral blood, bone-marrow cells, the spleen, and the liver 1 year after lentiviral-vector transduction.[24] These studies indicate that Farber disease and allelic disease(s) such as SMA-PME might be candidates for gene therapy in the near future. This underlines the importance of *ASAH1* or acid-ceramidase-activity screening in this subgroup of SMA-affected individuals for diagnosis and future therapeutics purposes.

Supplemental Data

Supplemental Data include one figure and one table and can be found with this article online at http://www.cell.com/AJHG/.

Acknowledgments

This work was supported by the Association Française contre les Myopathies (to J.M.; ref. 14383 and 13860), the Institut National de la Santé et de la Recherche Médicale (to J.M.), and Vaincre les Maladies Lysosomales (to T.L.). The authors would like to thank the Biomedical Institute of Bicêtre for providing us with Sanger-sequencing facilities, K. Sandhoff and H. Schulze (Bonn, Germany) for providing the rabbit anti-ceramidase antibody, and the National Heart, Lung, and Blood Institute Grand Opportunity (GO) Exome Sequencing Project and its ongoing studies, the Lung GO Sequencing Project (HL-102923), the Women's Health Initiative Sequencing Project (HL-102924), the Broad GO Sequencing Project (HL-102925), the Seattle GO Sequencing Project (HL-102926), and the Heart GO Sequencing Project (HL-103010), which all produced and provided exome variant calls for comparison. The authors wish to dedicate this work to the memory of C. Brahe, who recently passed.

Received: January 10, 2012
Revised: March 12, 2012
Accepted: May 1, 2012
Published online: June 14, 2012

Web Resources

The URLs for data presented herein are as follows:

BLAST, http://blast.ncbi.nlm.nih.gov/Blast.cgi

dbSNP, http://www.ncbi.nlm.nih.gov/snp
ESEfinder Release 2.0, http://rulai.cshl.edu/tools/ESE2/
Exome Variant Server, http://evs.gs.washington.edu/EVS/
Online Mendelian Inheritance in Man (OMIM), http://www.omim.org
PolyPhen-2, http://genetics.bwh.harvard.edu/pph2/

References

1. Lefebvre, S., Bürglen, L., Reboullet, S., Clermont, O., Burlet, P., Viollet, L., Benichou, B., Cruaud, C., Millasseau, P., Zeviani, M., et al. (1995). Identification and characterization of a spinal muscular atrophy-determining gene. Cell *80*, 155–165.
2. Jankovic, J., and Rivera, V.M. (1979). Hereditary myoclonus and progressive distal muscular atrophy. Ann. Neurol. *6*, 227–231.
3. Haliloglu, G., Chattopadhyay, A., Skorodis, L., Manzur, A., Mercuri, E., Talim, B., Akçören, Z., Renda, Y., Muntoni, F., and Topaloğlu, H. (2002). Spinal muscular atrophy with progressive myoclonic epilepsy: Report of new cases and review of the literature. Neuropediatrics *33*, 314–319.
4. Rüschendorf, F., and Nürnberg, P. (2005). ALOHOMORA: A tool for linkage analysis using 10K SNP array data. Bioinformatics *21*, 2123–2125.
5. Abecasis, G.R., Cherny, S.S., Cookson, W.O., and Cardon, L.R. (2002). Merlin—rapid analysis of dense genetic maps using sparse gene flow trees. Nat. Genet. *30*, 97–101.
6. Li, H., and Durbin, R. (2009). Fast and accurate short read alignment with Burrows-Wheeler transform. Bioinformatics *25*, 1754–1760.
7. Li, H., Handsaker, B., Wysoker, A., Fennell, T., Ruan, J., Homer, N., Marth, G., Abecasis, G., and Durbin, R.; 1000 Genome Project Data Processing Subgroup. (2009). The Sequence Alignment/Map format and SAMtools. Bioinformatics *25*, 2078–2079.
8. Wang, K., Li, M., and Hakonarson, H. (2010). ANNOVAR: Functional annotation of genetic variants from high-throughput sequencing data. Nucleic Acids Res. *38*, e164.
9. Bedia, C., Casas, J., Andrieu-Abadie, N., Fabriàs, G., and Levade, T. (2011). Acid ceramidase expression modulates the sensitivity of A375 melanoma cells to dacarbazine. J. Biol. Chem. *286*, 28200–28209.
10. Chatelut, M., Leruth, M., Harzer, K., Dagan, A., Marchesini, S., Gatt, S., Salvayre, R., Courtoy, P., and Levade, T. (1998). Natural ceramide is unable to escape the lysosome, in contrast to a fluorescent analogue. FEBS Lett. *426*, 102–106.
11. Medin, J.A., Takenaka, T., Carpentier, S., Garcia, V., Basile, J.P., Segui, B., Andrieu-Abadie, N., Auge, N., Salvayre, R., and Levade, T. (1999). Retrovirus-mediated correction of the metabolic defect in cultured Farber disease cells. Hum. Gene Ther. *10*, 1321–1329.
12. Bedia, C., Camacho, L., Abad, J.L., Fabriàs, G., and Levade, T. (2010). A simple fluorogenic method for determination of acid ceramidase activity and diagnosis of Farber disease. J. Lipid Res. *51*, 3542–3547.
13. Sabourdy, F., Labauge, P., Stensland, H.M., Nieto, M., Garcés, V.L., Renard, D., Castelnovo, G., de Champfleur, N., and Levade, T. (2009). A MANBA mutation resulting in residual beta-mannosidase activity associated with severe leukoencephalopathy: a possible pseudodeficiency variant. BMC Med. Genet. *10*, 84.
14. Bielawska, A., Perry, D.K., and Hannun, Y.A. (2001). Determination of ceramides and diglycerides by the diglyceride kinase assay. Anal. Biochem. *298*, 141–150.
15. Westerfield, M. (1995). The zebrafish book. A guide for the laboratory use of zebrafish (Danio rerio) (Eugene, OR: University of Oregon Press).
16. Nasevicius, A., and Ekker, S.C. (2000). Effective targeted gene "knockdown" in zebrafish. Nat. Genet. *26*, 216–220.
17. Adzhubei, I.A., Schmidt, S., Peshkin, L., Ramensky, V.E., Gerasimova, A., Bork, P., Kondrashov, A.S., and Sunyaev, S.R. (2010). A method and server for predicting damaging missense mutations. Nat. Methods *7*, 248–249.
18. Cartegni, L., Wang, J., Zhu, Z., Zhang, M.Q., and Krainer, A.R. (2003). ESEfinder: A web resource to identify exonic splicing enhancers. Nucleic Acids Res. *31*, 3568–3571.
19. Furutani-Seiki, M., Jiang, Y.J., Brand, M., Heisenberg, C.P., Houart, C., Beuchle, D., van Eeden, F.J., Granato, M., Haffter, P., Hammerschmidt, M., et al. (1996). Neural degeneration mutants in the zebrafish, Danio rerio. Development *123*, 229–239.
20. Melançon, E., Liu, D.W., Westerfield, M., and Eisen, J.S. (1997). Pathfinding by identified zebrafish motoneurons in the absence of muscle pioneers. J. Neurosci. *17*, 7796–7804.
21. Levade, T., Sandhoff, K., Schulze, H., and Medin, J.A. (2009). Acid Ceramidase Deficiency: Farber Lipogranulomatosis. In Scriver's OMMBID (The Online Metabolic & Molecular Bases of Inherited Disease), Valle, Beaudet, Vogelstein, Kinzler, Antonorakis, and Ballabio, eds. (McGraw-Hill), http://www.ommbid.com.
22. Samuelsson, K., and Zetterström, R. (1971). Ceramides in a patient with lipogranulomatosis (Farber's disease) with chronic course. Scand. J. Clin. Lab. Invest. *27*, 393–405.
23. Yeager, A.M., Uhas, K.A., Coles, C.D., Davis, P.C., Krause, W.L., and Moser, H.W. (2000). Bone marrow transplantation for infantile ceramidase deficiency (Farber disease). Bone Marrow Transplant. *26*, 357–363.
24. Walia, J.S., Neschadim, A., Lopez-Perez, O., Alayoubi, A., Fan, X., Carpentier, S., Madden, M., Lee, C.J., Cheung, F., Jaffray, D.A., et al. (2011). Autologous transplantation of lentivector/acid ceramidase-transduced hematopoietic cells in nonhuman primates. Hum. Gene Ther. *22*, 679–687.